# Single capsid mutations modulating phage adsorption, persistence, and plaque morphology shape evolutionary trajectories in ΦX174

Short title:

**Life history evolution in ΦX174**

Key words:
**Adsorption, persistence, ΦX174, lytic bacteriophage, phage therapy, phage evolution**

Manuela Reuter[1], Michael Sieber[1], Octavio Reyes-Matte[1], Christina Vasileiou[1], Christopher Böhmker[1], Jordan Romeyer Dherbey[2], Frederic Bertels[1,*] and Javier Lopez-Garrido[1,*]

[1]Max Planck Institute for Evolutionary Biology, Plön, Germany
[2]University of Cambridge, Cambridge, United Kingdom

*Correspondence: frederic.bertels.publications@gmail.com; lopezgarrido@evolbio.mpg.de

**Abstract**

The evolutionary success of lytic bacteriophages depends on key life-history traits, including adsorption, lysis time, burst size and persistence in the environment. However, how these traits evolve to allow adaptation to different environments remains poorly understood. Here, we explored this question in phage ΦX174, combining experimental evolution and mathematical modelling. By investigating how serial transfer conditions shape evolutionary outcomes in liquid culture, we found that the time between transfers imposes divergent selection on adsorption and context-dependent directional selection on persistence. Longer transfer intervals, which allow multiple infection cycles until host depletion, favoured fast-adsorbing, highly persistent mutants that could rapidly initiate infections and remained viable in the absence of the host. In contrast, shorter transfer intervals selected for slower adsorption without substantially altering persistence. Mathematical modelling of phage infection dynamics revealed that slow adsorption reduces the likelihood of irreversible phage attachment to already infected cells, thereby increasing the number of free phages able to initiate new infections upon dilution. These trade-offs resulted in distinct plaque phenotypes on solid media: fast adsorbers formed small plaques, while slow adsorbers formed large ones. A single-point mutation in the major capsid protein was sufficient to drive these changes in adsorption. In the case of fast-adsorbing mutants, this mutation was pleiotropic and also enhanced environmental persistence. Our findings show how simple changes in propagation conditions can steer phage phenotypes, providing insights relevant to evolutionary biology and phage therapy.

## Introduction

The success of lytic bacteriophages relies on four central life-history traits, each of which may evolve under different selective pressures to maximise fitness [1–6]. These traits are: (I) adsorption constant, which determines the ease with which a phage irreversibly attaches to a host cell, (II) latent period, or time required to complete the infection cycle inside the host, (III) burst size, defined as the number of new phage particles produced per infected host cell, and (IV) decay rate, representing the loss of infectious phage particles in the absence of susceptible host cells [7–12].

Interest in these traits has grown due to the need to predict phage virulence for medical and biocontrol applications [13–16]. However, such predictions remain challenging because the fitness effects of individual traits are often highly context-dependent [17–19]. For example, high adsorption rates are typically considered beneficial in well-mixed liquid environments, where they facilitate rapid infection initiation [20, 21]. However, in spatially-structured environments such as biofilms, these same traits can hinder phage spread to uninfected neighbouring cells by promoting phage attachment to already infected cells at the centre of infection [17, 22]. Understanding how life-history traits influence phage fitness across environments is therefore essential for predicting and potentially optimising phage performance.

The model coliphage ΦX174 provides a powerful platform for dissecting how the relationship between trait and environment impacts fitness. [23–27]. ΦX174 is a strictly lytic, tailless phage of the *Microviridae* family, best known as the first DNA-based organism whose entire genome was sequenced [28]. Its 5386 bp circular single-stranded DNA genome encodes only 11 genes, most of which are necessary for phage DNA replication, morphogenesis and host lysis [28–31]. Only four genes (F, G, H, and J) encode for proteins that form the mature virion [32, 33]. The icosahedral capsid is made of 60 F, 60 J and 12 H protein monomers, decorated at each of its 12 vertices by 5 G spike monomers [32, 34]. G likely mediates host recognition and subsequent attachment to host lipopolysaccharide (LPS), after which it dissociates, allowing F to bind irreversibly to the host cell surface [35–37]. Irreversible binding triggers a conformational change that results in the injection of phage DNA into the host cell through the pilot protein H [37, 38].

Here, we have explored how life-history traits influence phage fitness across different environments by evolving ΦX174 under contrasting serial transfer regimes. Through a combination of life-history trait quantification and mathematical modelling, we have identified individual mutations that alter adsorption constant and persistence, leading to fitness effects that are strongly dependent on the environment. By disentangling these context-dependent fitness effects, our results improve our understanding of phage ecology and evolution and also provide insights for rational trait optimisation in medical and biocontrol applications.

82 **Materials and Methods**

83 **Strains and culture conditions**

84 The ancestral ΦX174 and its host *E. coli* C were provided by H.A. Wichman
85 (Department of Biological Sciences, University of Idaho). All evolved phage strains were
86 derived from the same ΦX174 genotype (GenBank: AF176034). Cultures were grown in
87 Lysogeny Broth (LB, Miller) supplemented with 10 mM $MgCl_2$ and 5 mM $CaCl_2$ and incubated
88 at 37°C, shaking at 250 rpm (orbital shaking diameter 2.5 cm). Mid-exponential *E. coli* C
89 cultures (~$2*10^8$ colony-forming units [CFU] per ml) were prepared from overnight cultures
90 and used for all infection experiments.

91 **Preparation of phage lysates and quantification**

92 Phage lysates were generated as described in Romeyer Dherbey *et al*. [39] by infecting
93 exponentially growing *E. coli* C with ΦX174 for 3 hours. After 3 hours, the remaining bacteria
94 were removed with chloroform and subsequent centrifugation. Phage-containing supernatants
95 were collected and stored for assays at 4°C or at -80°C for long-term storage.

96 Phage titers were quantified by plaque assays in which plaque-forming units (PFUs)
97 were assessed by plating 100 µl of diluted phage lysate with 100 µl of *E. coli* C overnight
98 culture pre-mixed in 4 ml semi-solid agar (SSA, 0.5% agar, supplemented with 10 mM $MgCl_2$
99 and 5 mM $CaCl_2$). The mixture was overlayed on a plate of LB-agar (1.5%) and incubated at
100 37°C for 18 hours. Phage lysates were diluted in phage buffer juice (PBJ: 2.03% Tris-HCl,
101 0.61% $MgCl_2$).

102 **Serial transfer regimes**

103 For every transfer regime, five independent selection lines were initiated by infecting
104 mid-exponential phage-sensitive *E. coli* C cultures with individual ancestral ΦX174 extracted
105 from independent plaques. Consecutive transfers were inoculated from phage lysate at $MOI_{input}$
106 ~0.1. The 3-hour regime involved 3-hour infections followed by chloroform phage extraction.
107 Serial transfers continued until heritable small-plaque mutants emerged, which were isolated
108 and replated multiple times to confirm the phenotype. The 30-min regime involved four daily
109 30-minute transfers followed by one 3-hour amplification step, repeated for ten days.
110 Individual plaques were isolated at the end for sequencing. An additional line was propagated

using only 30-minute transfers, without the amplification step. Phages were extracted with chloroform and transferred after each round at $MOI_{input}$ ~0.1 for 40 passages. Population sequencing was used to monitor mutation dynamics. Additional details can be found in **Fig. S1 and Supplementary Methods**.

**Sanger sequencing of evolved phages**

Whole-genome Sanger sequencing was conducted for individual phage isolates from both transfer regimes according to Biggs *et al*. [40]. DNA was extracted from high-titer lysates (QIAprep Spin Miniprep Kit® Qiagen, Hilden, Germany) and amplified via PCR in two genome halves. PCR products were purified (QIAprep PCR Purification Kit® Qiagen, Hilden, Germany) and sequenced at the Max Planck Institute for Evolutionary Biology. Primers and settings used for amplification and sequencing are in **Tables S1, S2, and S3**. Sequences were aligned against the reference ΦX174 genome using Geneious Prime 2023.0.1 (https://www.genious.com). Identified amino acid positions in which single-point mutations were located were numbered by including the start codon as position one [39].

**Adsorption assays**

Adsorption constants were determined following a modified version of the Hyman and Abedon assay [41]. Mid-exponential, phage-sensitive *E. coli* C cultures were infected with phages at $MOI_{input}$ ~0.05 at 37°C in a shaking water bath at 200 rpm. Phages were sampled 2, 4, and 6 minutes post-infection and diluted 10-fold into non-supplemented LB. Samples were cooled on ice to stop infection, treated with chloroform, and quantified. Adsorption constants were calculated by fitting linear models to log-transformed phage titers and dividing slope estimates by bacterial density. Differences between genotypes were tested using a linear mixed model (replicate as random effect) and post hoc Tukey tests for multiple comparisons (**Supplementary Methods**).

**Phage persistence assays**

Persistence was measured over a 5-hour infection period. An exponentially-growing *E. coli* C culture was infected at $MOI_{input}$ ~0.1, and samples were taken every 30 minutes. Mature phages were extracted with chloroform, and phage titers were determined by PFU counting.

Decay rates were estimated by fitting exponential decay models to the titer decline period after peak productivity. Model fitting procedures are detailed in **the Supplementary Methods**.

**Simulations of phage evolution**

The following system of delay differential equations (DDEs) describes the dynamics of the bacterial host $B$ (cells per ml), the infected bacterial population $B_I$ (cells per ml), and the three phage types $P_A$ (ancestral, particles per ml), $P_L$ (large-plaque type, particles per ml), and $P_S$ (small-plaque type, particles per ml). In addition,$B_\tau = B(t-\tau)$denotes the bacterial density$\tau$minutes in the past, reflecting the delay introduced by the lysis time. We use a similar notation for the phage densities, e.g. $P_{A,\tau}$denotes the density of the ancestral phage $\tau$minutes in the past.

Bacterial growth throughout the transfer period was found not to play a significant role in the simulations, so it is neglected in the model for simplicity. All parameter values and their biological meaning are given in **Table 1** in the main text.

$$\frac{dB}{dt} = -(\phi_A P_A + \phi_L P_L + \phi_S P_S)B$$

$$\frac{dB_I}{dt} = \phi_A\left(BP_A - B_\tau P_{A,\tau}\right) + \phi_L\left(BP_L - B_\tau P_{L,\tau}\right) + \phi_S\left(BP_S - B_\tau P_{S,\tau}\right)$$

$$\frac{dP_A}{dt} = \phi_A\left((1-m)\beta B_\tau P_{A,\tau} - (B+B_I)P_A\right) + \frac{1}{2}m\beta B_\tau\left(\phi_L P_{L,\tau} + \phi_S P_{S,\tau}\right) - \delta_A P_A$$

$$\frac{dP_L}{dt} = \phi_L\left((1-m)\beta B_\tau P_{L,\tau} - (B+B_I)P_L\right) + \frac{1}{2}m\beta B_\tau\left(\phi_A P_{A,\tau} + \phi_S P_{S,\tau}\right) - \delta_L P_L$$

$$\frac{dP_S}{dt} = \phi_S\left((1-m)\beta B_\tau P_{S,\tau} - (B+B_I)P_S\right) + \frac{1}{2}m\beta B_\tau\left(\phi_A P_{A,\tau} + \phi_L P_{L,\tau}\right) - \delta_S P_S$$

The DDE system was solved numerically in Python using the *scipy*-based *ddeInt* solver. After 30 minutes or 3 hours of simulated time, depending on the transfer regime, the system was reset to the initial density of fresh bacteria $B$ ($10^8$ CFU), and 2% of the final densities of infected bacteria $B_I$ and all three phage types, respectively. This starts the next growth cycle and corresponds to the transfer protocol of the experiment.

160 **Table 1: Parameters and corresponding parameter values used in the mathematical model.**

| Parameter | Value |
|---|---|
| Adsorption constant, ancestor | $4.15*10^{-9}$ ($ml^{-1}$ min-1) |
| Adsorption constant, large-plaque type | $9.87*10^{-10}$ ($ml^{-1}$ min-1) |
| Adsorption constant, small-plaque type | $6*10^{-9}$ ($ml^{-1}$ min-1) |
| Burst size, all types | 200 (per infected host cell) |
| Lysis time, all types | 17 min |
| Decay rate, ancestor | $1.7*10^{-2}$ ($min^{-1}$) |
| Decay rate, large-plaque type | $1.4*10^{-2}$ ($min^{-1}$) |
| Decay rate, small-plaque type | $6*10^{-3}$ ($min^{-1}$) |
| Mutation rate | $10^{-5}$ (per minute) |

161

162 **Image analysis of lysis plaques**

163 Lysis plaque morphology was quantified using a custom image analysis pipeline.
164 Plaques were imaged under standardised conditions (ChemiDoc: Bio-Rad, California, USA;
165 0.1s exposure time) and processed using Ilastik [42] for pixel classification based on intensity,
166 texture, and edge features. Post-processing steps included erosion, whole-filling, and
167 watershed transformation using SciPy [43] and scikit-image [44]. Each plaque was assigned
168 an ID and analysed for area ($cm^2$), distance to periphery (via distance transform) and grayscale
169 intensity (overlaying mask on original image) (details see **Supplementary Methods**).

170 **Data analysis and visualisation**

171 Statistical analysis of adsorption constants, model fitting for adsorption and decay and
172 all data visualisations were performed in R (version 4.2.1) [45]. Details of the packages are
173 found in **Table S13**. The protein structure, resolved by McKenna *et al*. [32], shown in **Fig. 5A**,
174 was taken from RCSB PDB (reference 2BPA:
175 https://www.wwpdb.org/pdb?id=pdb_00002bpa), and the mutation visualisation was done in
176 UCSF Chimera (version 1.18). All cartoons were created using BioRender® as indicated in the
177 corresponding figure legends.

178

## Results

### Differences in transfer intervals during serial passaging drive the evolution of contrasting lysis plaque phenotypes

In the context of a previous study [39], we observed that small and turbid plaques frequently emerged when ΦX174 was serially transferred after 3-hour incubation periods with host cells in liquid culture. To confirm this observation, we evolved multiple independent selection lines of the ancestral ΦX174 under the same selection regime (hereafter, 3-h regime) and plated the evolving phage populations onto lawns of phage-sensitive host cells at every transfer (**Fig. 1; Fig. S1A**). Small, turbid plaques appeared in all lines after four to seven transfers (**Fig. 1; Fig. S2**).

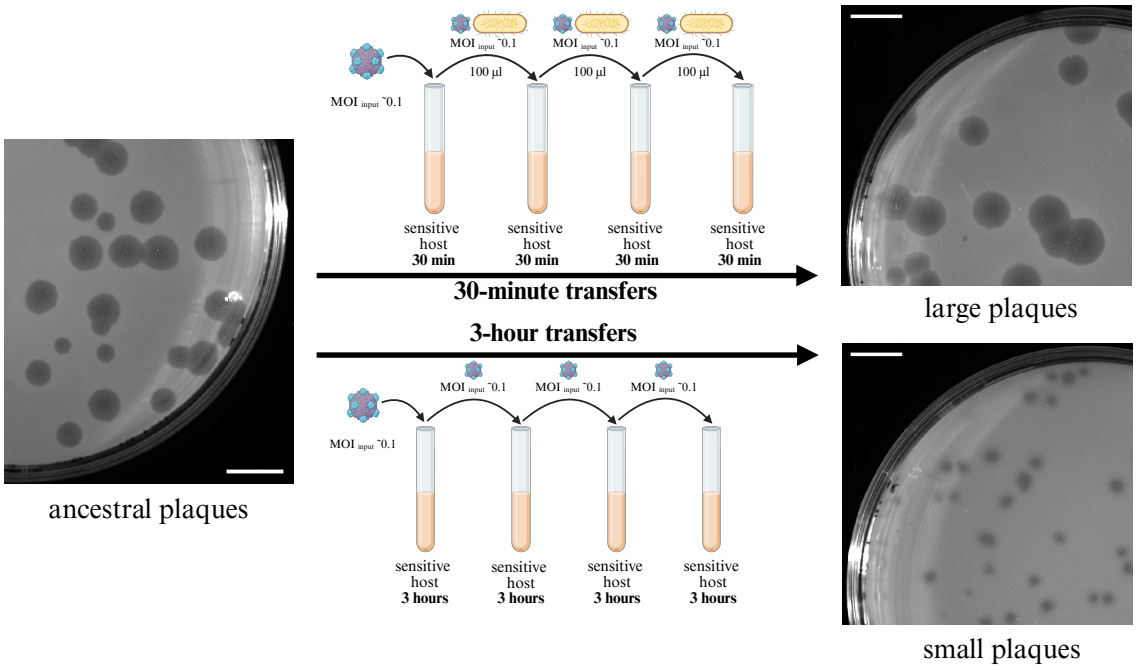


**Fig. 1: 30-min and 3-h transfer regimes select for large- and small-plaque-forming phages, respectively.** Phage ΦX174 was propagated under 30-min (top) or 3-h (bottom) regimes, leading to the evolution of large- and small-plaque-forming phages, respectively. Ancestral plaques are shown on the left, and evolved large (top) and small (bottom) plaques on the right. Scale bars, 1 cm. All plaque images have the same magnification. Diagrams of the 30-min and 3-h regimes are in the middle. The approximate input multiplicity of infection ($MOI_{input}$) and incubation times are the same for each transfer. For illustration purposes, only four transfers are shown, but the experiment involved more transfers. See methods and **Fig. S1** for details. Figure was created in BioRender. Reuter, M. (2025) https://BioRender.com/20imrdd.

202 Since differences in plaque morphology often reflect underlying changes in life history
203 traits [2, 17, 22, 46–48], we hypothesised that our experimental regime was selecting for phages
204 with changes in one or more life history traits. The 3-h regime provides sufficient time for
205 phages to complete multiple infection cycles, potentially depleting host cells and altering
206 selective pressures. To test whether transfer length affects plaque phenotype evolution, we
207 performed a second evolution experiment in which phages were serially transferred every 30
208 minutes (hereafter, referred to as the 30-min regime) (**Fig. 1, Fig. S1B**), a timeframe during
209 which most phages can complete only a single infection cycle (**Fig. S3**). In contrast to the 3-h
210 transfer regime, no small plaques were detected under the 30-min regime, even after 40
211 transfers (**Fig. 1**). However, to our surprise, we began to observe plaques larger than those
212 formed by the ancestral phage after approximately 20 transfers (**Fig. 1; Fig. S2**).
213
214 **Large- and small-plaque phenotypes are caused by different mutations in the major**
215 **capsid (F) protein**
216 To identify the genetic modifications leading to the small- and large-plaque phenotypes,
217 we isolated five phages of each type, one per selection line, and sequenced their genomes. Each
218 evolved isolate differed from the ancestor by only one or two single-point mutations (**Fig. 2**).
219
220 All five large-plaque mutants isolated from the 30-min regime lines carried an A-to-G
221 transition at position 1301 in the phage genome, resulting in a threonine-to-alanine substitution
222 at position 101 of the F gene [A1301G/F(T101A)] (**Fig. 2A**). The mutant isolated from line 3
223 carried only this substitution. The other four isolates carried one additional mutation in either
224 the F or the H protein (**Fig. 2A**) acquired after the F(T101A) mutation (see Sanger Sequencing,
225 Zenodo: 10.5281/zenodo.17076221). Phenotypically, however, all large-plaque mutants
226 resembled each other (**Fig. 2A, Fig. S4**), suggesting that the T101A mutation in the F protein
227 is sufficient for the manifestation of the large-plaque phenotype.
228
229 None of the mutations observed in large-plaque mutants were found in the small-
230 plaque-forming phages isolated from the 3-h regime lines. However, all five small-plaque
231 phages also differed from the ancestor by a single-point mutation in the F gene (**Fig. 2B**), each
232 producing a distinct small-plaque phenotype (**Fig. 2B and S4**). The most drastic phenotype
233 was caused by the G1965A/F(G322D) mutation, resulting in the formation of extremely small
234 and turbid plaques. Phages carrying the C2280A/F(S427*) mutation, which truncates the major
235 capsid protein by the last amino acid, produced slightly larger and clearer plaques (**Fig. S4**).

The G1639A/F(M213I) mutation led to a heterogeneous phenotype, with both small and large plaques, and was excluded from further analysis.

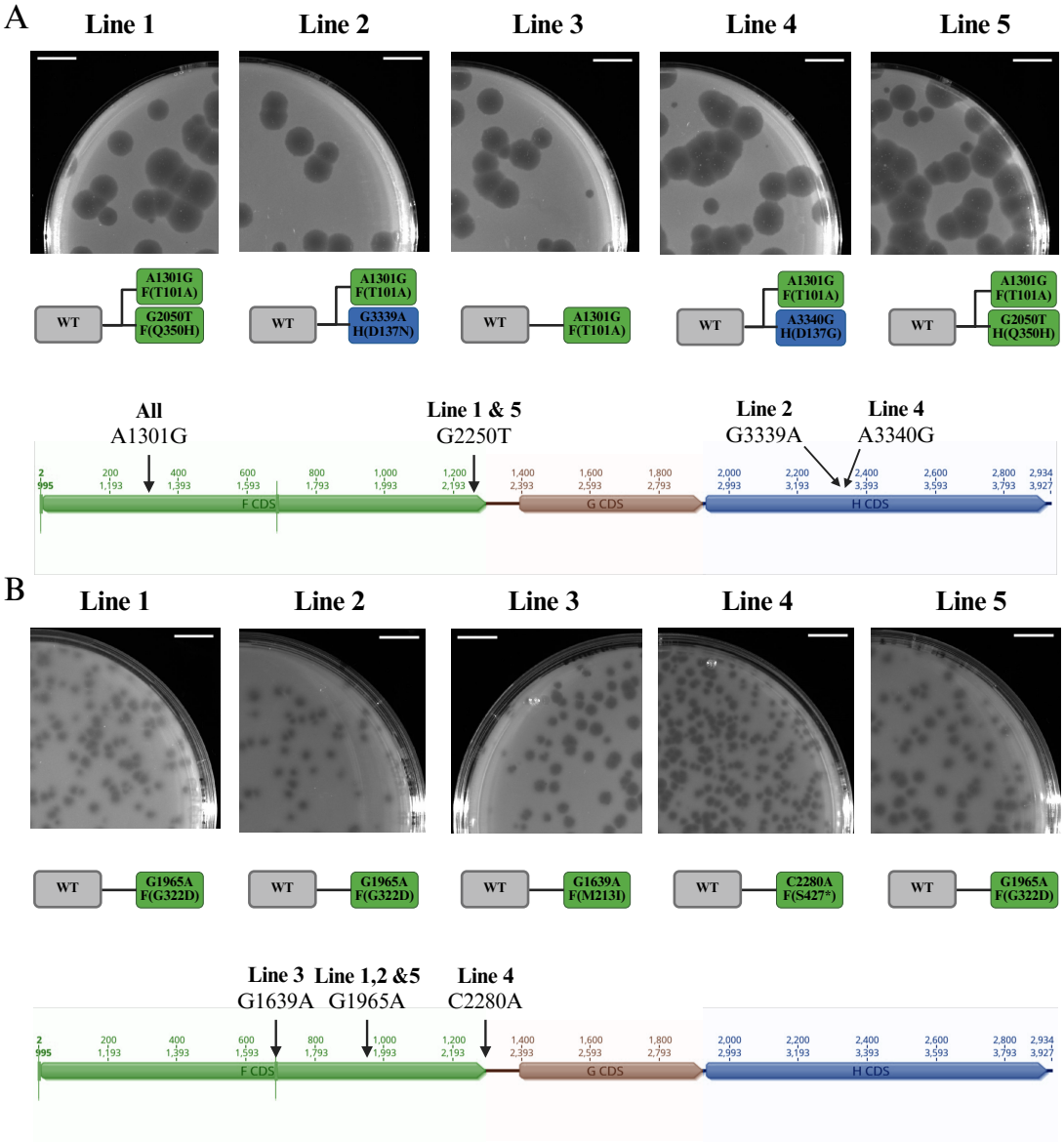


**Fig. 2: Mutations linked to large- and small-plaque phenotypes occur in the major capsid protein.** (A) Large-plaque phenotypes (top) and corresponding genotypes (bottom) of mutants isolated from independent lines of the 30-min regime. All the mutants carried an A-to-G transition at position 1301 (A1301G) in the phage genome, resulting in a threonine-to-alanine substitution at position 101 of the F protein [F(T101A)]. Four isolates carried an additional mutation, either in the F (green) or the H (blue) gene. The ancestor is shown in grey (WT). (B) Small-plaque phenotypes (top) and genotypes (bottom) of mutants isolated from independent lines of the 3-h regime. All mutants differed from the ancestor by different mutation in the F gene (green), resulting in different amino acid changes: G322D in the clones from lines 1, 2 and 5; M213I in the clone from line 3; and the formation of a premature stop codon at the very last codon of the F gene (S427*) in the clone from line 4. The nucleotide change in the phage genome is shown at the top, and the corresponding amino acid change at the bottom. The ancestor is shown in grey (WT). Scale bars, 1 cm. Genome illustrations were generated using Geneious Prime 2023.0.1. Figure created in BioRender. Reuter, M. (2025) https://BioRender.com/du5tsj2.

251 Altogether, the sequencing results indicate that different modifications of the major
252 capsid protein are responsible for the contrasting plaque phenotypes emerging in our selection
253 regimes.
254
255 **Plaque size negatively correlates with the adsorption constant**
256 The major capsid protein is likely essential for the irreversible adsorption of ΦX174 to
257 the host cells [37], suggesting the large- and small-plaque-forming phages may have evolved
258 different adsorption constants compared to the ancestral ΦX174. To test this hypothesis, we
259 measured the adsorption constant of the ancestral phage, a large-plaque-forming mutant
260 carrying the single F(T101A) mutation, and the two small-plaque mutants, F(G322D)
261 and F(S427*). We focused on mutants with single substitutions to ensure that each mutation
262 could be directly linked to specific changes in life history traits.
263
264 The adsorption constants of the evolved phages differed significantly from that of the
265 ancestral ΦX174 and correlated inversely with plaque size (**Fig. 3**). The ancestral mean
266 adsorption constant was $4.15 \times 10^{-9}$ $ml^{-1}$ $min^{-1}$ (**Table S4**), in close agreement with previous
267 estimations [49, 50]. The adsorption constants of the small-plaque-forming mutants were
268 slightly but significantly higher than the ancestral. Conversely, the large-plaque mutant had an
269 absorption rate constant approximately five-fold lower than the ancestral (**Table S4**).
270
271 The relationship between adsorption constant and plaque size was not linear. The large-
272 plaque mutant with a five-fold reduction in adsorption constant produced plaques that were
273 1.5-fold larger than those of the ancestor, whereas the small-plaque mutants with less than two-
274 fold increase in adsorption constant formed plaques about 10 times smaller (**Table S4**). These
275 results are in line with previous predictions of a non-linear relationship between adsorption
276 constant and plaque size [48].
277
278 These results demonstrate that the adsorption constants evolved in opposite directions
279 under the 3-h and 30-min regimes, and suggest that the differences in plaque size may be caused
280 by variation in phage-host cell binding affinity.

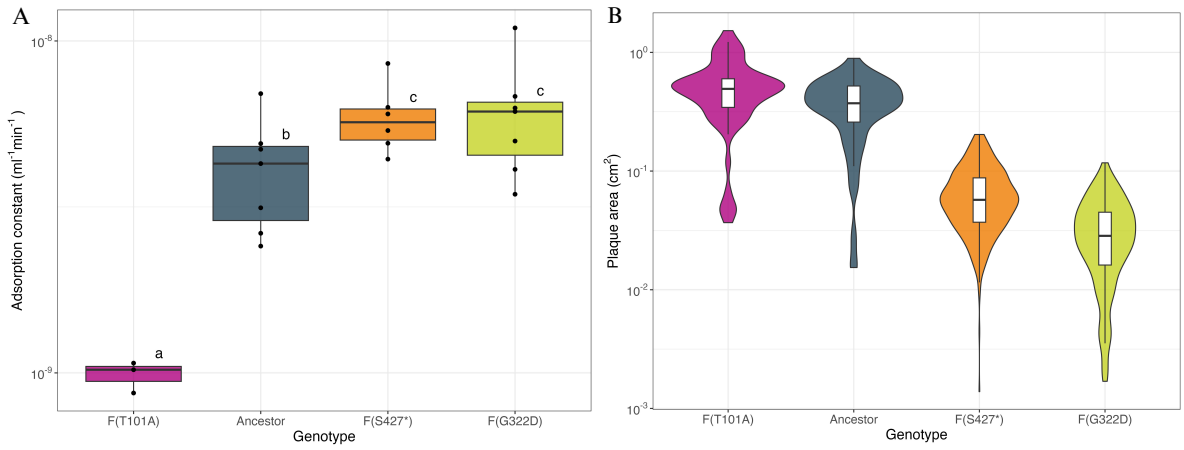


**Fig. 3: The adsorption constant is inversely correlated with plaque size.** (A) Adsorption constant "k" of the ancestor (grey), the large-plaque mutant F(T101A) (purple) and the two small-plaque mutants F(G322D) (orange) and F(S427*) (green). At least three independent experiments were performed for each genotype. Each black dot represents the adsorption constant of an individual experiment, the horizontal lines indicate the median, and the boxes span the middle 50% of the data. The whiskers span the lower and upper 25% of the data. Different letters on top of the boxes indicate significant adsorption constant differences between genotypes (significance level $p<0.05$). (B) Lysis plaque area in $cm^2$ (y-axis) for the ancestor (grey, n=76), and the evolved phages F(T101A) (purple, n=60), F(G322D) (green, n=303) and F(S427*) (orange, n=431). Violin plots show distribution shape; boxplots display medians (black lines), interquartile range (boxes), and upper/lower 25% (whiskers). See **Methods** and **Supplementary Methods** for details of adsorption and plaque phenotype analysis.

## Fast adsorption is detrimental in the 30-min regime

We expected fast adsorption to be beneficial in the well-mixed liquid environment in which our experimental evolution regimes took place, as it would allow rapid infection of host cells [20, 21]. Hence, we were surprised that phages with dramatically reduced adsorption constants were selected under the 30-min regime. To further explore the role of absorption rate in phage fitness under different transfer intervals, we developed a mathematical model of phage infection dynamics (**Fig. 4**).

The model captures the interaction between the bacterial host, the ancestral phage, the slow-adsorbing mutant, and the fast-adsorbing mutant during the transfer experiments. Upon adsorption of a phage to an uninfected host cell, the cell moves into the infected class. Phages of all types keep adsorbing to already infected cells, but only phages corresponding to the type that infected first are released upon lysis. We explicitly consider the lysis time, reflecting the time delay between adsorption of a phage and lysis of the infected cell, triggering the release of new viral particles. The full model is given in the **Supplementary Methods**.

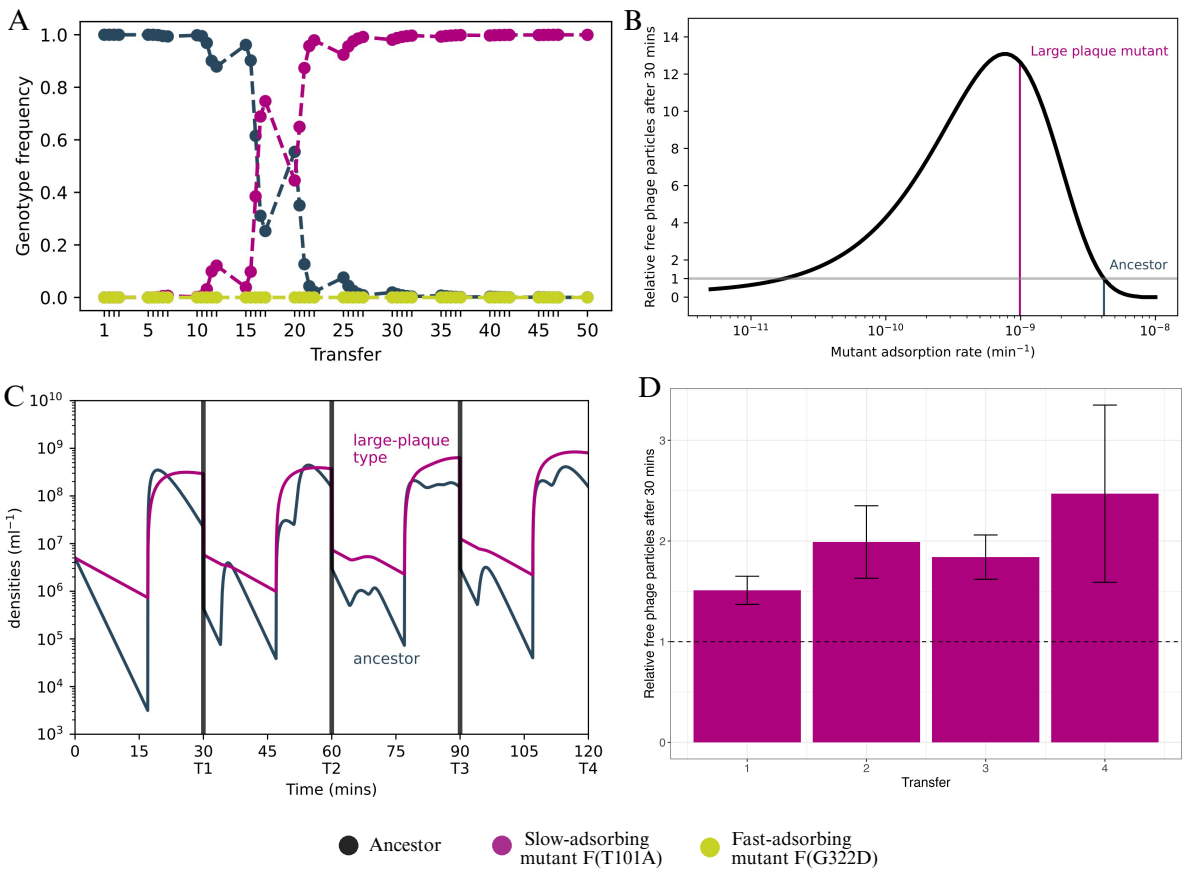


**Fig. 4: Simulations of the 30-min regime.** (A) Simulated dynamics of free phage populations (y-axis) across serial transfers (x-axis) in the 30-min regime, using genotypes with experimentally measured adsorption constants (green: mutant F(G322D); purple: mutant F(T101A); grey: ancestor). The simulation predicts the rapid emergence of the low-adsorption mutant, in line with experimental results. (B) Predicted optimal adsorption constants based on simulated competitions between the ancestor and hypothetical mutants with lower adsorption constants (x-axis), starting from an initial 1:1 ratio. The y-axis shows the predicted mutant-to-ancestor titer ratios after one transfer. The evolved mutant (purple line) closely matches the predicted optimum. (C) Simulation of free phage densities (y-axis) within four (T1-T4) 30-min transfer (x-axis) for the ancestor (grey) and large-plaque mutant F(T101A) (purple). The free phage dynamics within one transfer predict a higher number of free phages of the low-adsorption genotype F(T101A) at the end of a transfer. The high loss of comparably fast-adsorbing ancestral phages to dead-end adsorption at the moment of transfer results in the selection of mutant F(T101A). (D) Bar chart of experimentally measured free phages of mutant F(T101A) (purple bars) relative to ancestral free phages (y-axis) after a 30-min transfer for a total of four transfers (x-axis). The number of free phages of mutant F(T101A) was normalised for the free phages of the ancestor, here indicated by the dashed black line. The height of the bar represents the mean of three independent biological replicates, with error bars indicating the standard error.

We started the *in silico* transfer experiments with phages with the ancestral adsorption constant. We allowed for the appearance of mutations that increased or decreased the adsorption constant to the values measured experimentally for the fast-adsorbing mutant F(G322D) and the slow-adsorbing mutant F(T101A), respectively. All other life-history traits

329 were held constant (**Table 1**). The simulations predicted the evolution of the slow-adsorbing
330 mutant under the 30-min regime within a timescale compatible with our experimental
331 observations (**Fig. 4A; Fig. S2**). Note that the 30-min transfer regime was interrupted by a 3-h
332 incubation step after every fourth transfer to amplify the phage population (see Materials
333 &Methods, **Fig. S1**). Although this step slowed down the increase in the frequency of slow-
334 adsorbing mutants, it did not prevent their eventual fixation in the simulations.
335
336 To further investigate the benefit of low adsorption constants during 30-min transfers,
337 we simulated competition between the ancestral phage and hypothetical mutants with
338 adsorption constants ranging from the ancestor value to 1000-fold lower (**Fig. 4B**). Each
339 simulation began with a 1:1 ratio of ancestral and mutant phages at an input multiplicity of
340 infectiousness ($MOI_{input}$) of 0.1, and predicted the relative mutant titer after a single 30-min
341 transfer. The results revealed an optimal adsorption constant approximately 6-fold lower than
342 that of the ancestor, very close to the value observed in the F(T101A) mutant. Mutants with
343 very low adsorption constants were predicted to perform poorly due to limited infection
344 initiation, whereas mutants with very high adsorption constants were expected to also perform
345 poorly, as their rapid binding to host cells increased the risk of multiple attachment to one host
346 cell, resulting in a high number of phages being lost to "dead-end" infections.
347
348 A detailed analysis of the simulations revealed that, in the 30-min regime, the phage
349 adsorption constant influenced the number of free phages present at the moment of transfer
350 (**Fig. 4C**). For fast-adsorbing phages, the model predicted that a large fraction of phages would
351 be lost to dead-end adsorptions after the first infection cycle, due to a rapid MOI increase. In
352 contrast, slow-adsorbing phages remained largely unbound, resulting in a higher proportion of
353 free phages at the moment of transfer. This was beneficial, as free phages could readily infect
354 sensitive host cells in the subsequent cycle. Quantification of free phages using sterile filtration
355 after each 30-min transfer confirmed these predictions. The number of free phages was
356 consistently higher for slow-adsorbing mutants, whose adsorption constants were closer to the
357 simulated optimum, than for ancestral phages (**Fig. 4D**). These results indicate that reduced
358 adsorption constants can increase phage fitness under the 30-min regime by increasing the pool
359 of phages available to initiate new infections in the next cycle.
360
361
362

363 **3-h transfers select for high persistence outside the host**

364 In contrast to the 30-min regime, simulation under the 3-h regime predicted the eventual
365 evolution of fast-adsorbing, small-plaque mutants, consistent with our experimental
366 observations (**Fig. S5**). However, the predicted timescale was substantially longer than that
367 observed experimentally (**Fig. S2**). This suggests that, although increased adsorption was
368 beneficial in the 3-h regime, selection on adsorption alone was insufficient to explain the
369 evolution of the observed mutants.

370

371 To get insight into which additional life history traits might promote the rapid selection
372 of small-plaque mutants under the 3-h regime, we mapped the mutations underpinning the
373 small- and large-plaque phenotypes onto the ΦX174 F-protein structure. The large-plaque-
374 forming F(T101A) substitution was located in the centre of the F monomer. However, the two
375 small-plaque-associated mutations, F(G322D) and F(S427*), were at the peripheral interfaces
376 between F monomers in the assembled capsid (**Fig. 5A)**. These peripheral mutations might
377 influence capsid symmetry or stability by altering inter-subunit interactions, potentially
378 contributing to the persistence of small-plaque-forming mutant phages during extended
379 incubation periods.

380

381 To test this, we performed time-course infections using the ancestral ΦX174, the large-
382 plaque mutant, and the two small-plaque mutants. Infections were initiated at an $MOI_{input}$ of
383 ~0.1, and infectious phage titers were quantified at regular intervals over five hours following
384 chloroform extraction. All populations exhibited an initial production phase, during which
385 phage particles increased, followed by a decay phase after the depletion of susceptible host
386 cells (**Fig. S6**). The production period differed slightly between the different phages. The
387 ancestor and the large-plaque-forming mutant reached their maximum phage titer ~60 minutes
388 post-infection, with a ~5,000-fold increase in population size. Small-plaque mutants peaked
389 slightly later but achieved a 10,000-fold increase in population size. The higher population size
390 peak of small-plaque mutants may be attributed to their higher adsorption constant, allowing
391 for earlier infection initiation. The most striking differences, however, were observed during
392 the decay phase (**Fig. 5B**). Both the ancestor and the large-plaque-forming mutant showed a
393 drastic reduction in infective phage particles, with titers declining more than 15-fold by the end
394 of the experiment. In contrast, the small-plaque mutants maintained a relatively constant
395 number of infective particles throughout the remainder of the assay, showing only a minor
396 decline over time.

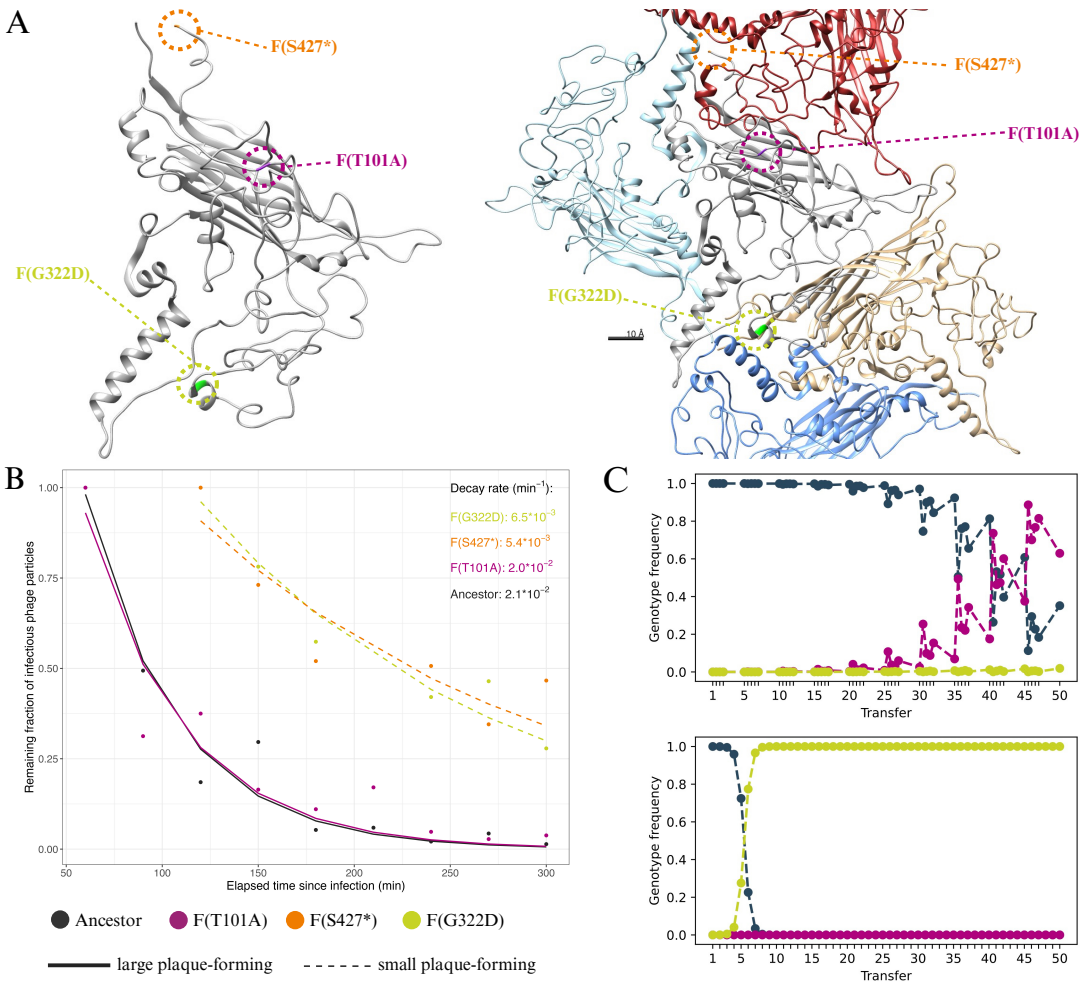


**Fig. 5: Single-point mutations in the major capsid protein modulate adsorption and persistence.** (A) Location of point mutations linked to plaque size differences in the F protein monomer (left) or multimer (right) structure. Mutations F(G322D) and F(S427) leading to small plaque phenotypes are shown in green and orange, respectively. Mutation F(T101) leading to a large plaque phenotype is shown in purple. Mutations associated with the small plaque phenotype are localised at monomer-monomer interfaces, whereas mutation F(T101) is located at the F protein centre. The protein structure, resolved by McKenna *et al*. [32], was taken from RCSB PDB (reference 2BPA: https://www.wwpdb.org/pdb?id=pdb_00002bpa). The figure was prepared in UCSF Chimera (version 1.18). (B) The y-axis shows the ratio of remaining particles relative to peak titer for the ancestor (grey), large-plaque mutant T101A (purple), and small-plaque mutants G322D (green) and S427* (orange). One experimental run, representative of multiple replicates, is shown. See **Supplementary Methods** for model selection and parameter extraction. (C) Simulations of free phage population dynamics (y-axis) across transfers (x-axis) for the 30-min (top) and 3-h (bottom) regimes, incorporating measured adsorption and decay for the ancestor (grey), T101A (purple), and G322D (green). Including decay improved prediction accuracy, especially under 3-h conditions, where it predicted the correct timing of small-plaque mutant evolution.

414 To test if differences in decay rates could explain the rapid evolution of the small-
415 plaque mutants in the 3-h regime, we incorporated the experimentally observed decay
416 parameters into our in silico serial transfer model (**Table 1**). In this case, the model predicted
417 the emergence of small-plaque mutants with enhanced persistence on a timescale consistent
418 with experimental observations (**Fig. 5C**). In contrast, adding persistence to simulations of the
419 30-min regime had minimal impact, slightly extending the predicted fixation time of the large-
420 plaque mutant and improving alignment with experimental observations (**Fig. 4A; Fig. 5C and**
421 **Fig. S2**).
422

423 **Discussion**

424 Our results reveal context-dependent fitness effects of persistence and adsorption in
425 ΦX174, modulated by the transfer time in serial passaging experiments. Lower adsorption
426 constants increase fitness under short transfer times. In contrast, longer transfer times select for
427 phages with higher adsorption constants and greater ability to persist outside the host.
428
429 These patterns can be explained by the ecological dynamics specific to each regime
430 (**Fig. 6**). In the 3-h regime, multiple infection cycles can occur per transfer. Fast-adsorbing
431 phages initiate these cycles more efficiently. Moreover, since phage populations increase by
432 more than two orders of magnitude per infection cycle (**Fig. S3**) and transfers are performed at
433 an $MOI_{input}$ of ~0.1 phages per bacterial cell, the vast majority of sensitive host cells are lysed
434 after two or three cycles, forcing phages to persist in the absence of host cells for extended
435 periods before being supplied with new susceptible hosts (**Fig. S6**). Thus, both enhanced
436 adsorption and environmental persistence are selected in this regime.
437
438 In contrast, under the 30-min regime, host cells are not exhausted between transfers.
439 Here, fast-adsorbing phages are more likely to adsorb to already infected cells (**Fig. 4**), leading
440 to unproductive infections due to superinfection inhibition or intracellular resource competition
441 [11, 40, 51]. Our simulations show that in these conditions, the early and frequent initiation of
442 infections by fast-adsorbing phages does not offset the losses incurred from unproductive
443 adsorption events (**Fig. 4C**). In contrast, slow-adsorbing phages are less likely to attach to
444 already infected cells and are more prone to being transferred as free phages. Upon transfer,
445 they encounter a fresh pool of uninfected hosts, allowing them to initiate productive infections
446 and outcompete their fast-adsorbing counterparts (**Fig. 6**). These findings challenge the
447 common assumption that high adsorption constants are universally advantageous in well-
448 mixed environments [20, 21].
449
450 Both adsorption and persistence are influenced by mutations in the major capsid protein
451 F, which likely plays a key role in irreversible adsorption to the host cell [32, 37]. The T101A
452 substitution, associated with a low adsorption constant, is located in an α-helix at the centre of
453 the F protein. Previous studies have identified this region as key to host specificity and binding
454 affinity [23, 25, 27, 39, 52, 53]. For example, Pepin *et al*. [53] identified a threonine-to-serine
455 substitution in the same residue that enabled phages to infect host cells with modified LPS.
456 Similarly, Crill *et al*. [25] described a glycine-to-aspartate substitution at position 102 that

457 drastically reduced adsorption to *E. coli* C but increased binding affinity to *Salmonella*,
458 highlighting the role of this region in attachment to the host.

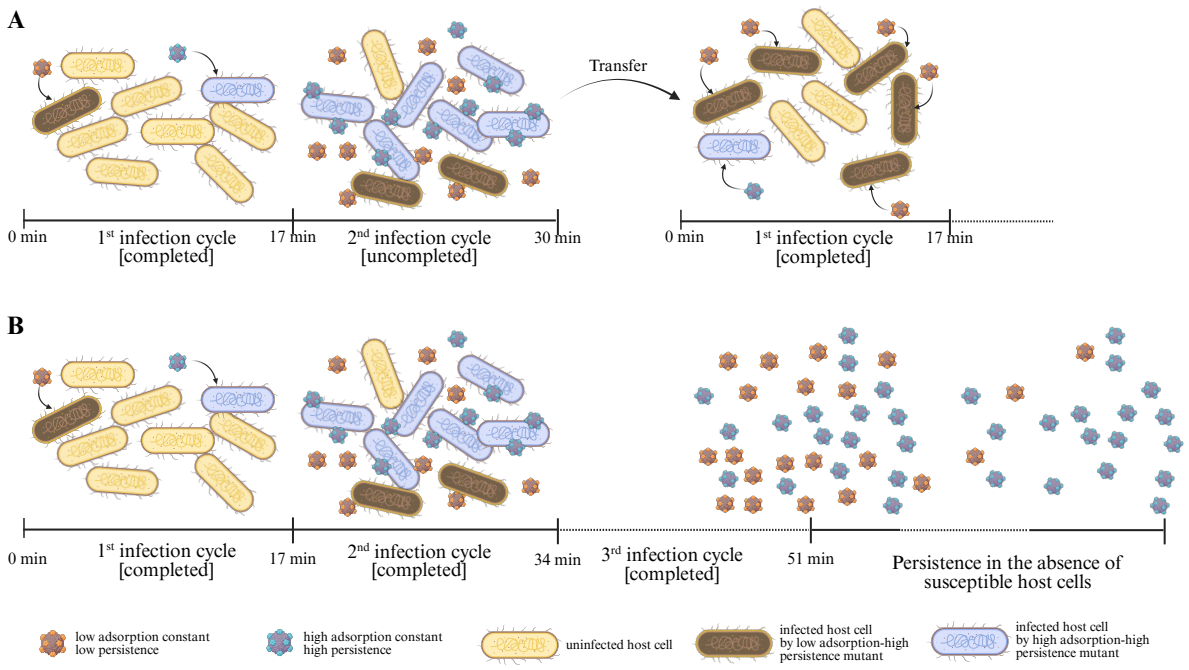


459

460 **Fig. 6: Schematic overview of phage population dynamics during 30-min and 3-h transfers.** In both panels,
461 low-adsorption and -persistence phages are shown in orange and corresponding infected host cells in brown. High-
462 persistence and -adsorption phages in blue and their infected hosts in light blue. Uninfected hosts are shown in
463 yellow. (A) In the 30-min regime, mutants with low adsorption constants (orange) are selected, as they are
464 transferred at high rates as free phage particles due to their delayed adsorption. Free phages can immediately
465 initiate new infection cycles when they are transferred to fresh, phage-sensitive hosts. In contrast, phages with
466 high adsorption constants have a lower chance of being transferred as free phage particles and engage in
467 unproductive infections by attaching to already infected cells. (B) In the 3-h regime, phages are left without
468 susceptible host cells (persistence period) after 2-3 infection cycles (growth period). High persistence phage
469 mutants, which also have a high adsorption constant, are selected under these conditions due to both their faster
470 adsorption and slower decay. In this case, high adsorption is beneficial as it allows phages to more effectively
471 scavenge sensitive host cells. Figure created in BioRender. Reuter, M. (2025) https://BioRender.com/xvtmw9p.

472

473 Two additional F mutations, both located at the monomer-monomer interface in the
474 assembled capsid (**Fig. 5A**), increased adsorption and dramatically increased persistence.
475 Changes in this region can affect capsid symmetry and stability in icosahedral phages [54, 55].
476 The pleiotropic nature of these mutations makes it difficult to disentangle the relative fitness
477 contributions of adsorption and persistence. However, the drastic increase in persistence
478 compared to the modest elevation in the adsorption constant suggests that persistence is the
479 primary trait under selection. This is further supported by our simulations, which show that

480 although both increased adsorption and persistence are favoured under the 3-h regime (**Fig.**
481 **5C**), selection on persistence alone leads to a more rapid evolution of small-plaque mutants
482 than selection on adsorption alone (**Fig. S5**).
483
484 Plaque phenotypes mirrored the contrasting selective pressures in our experiments, with
485 small- and large-plaque-forming phages evolving under the 3-h and 30-min regimes,
486 respectively. These differences in plaque size may reflect adsorption differences, as we found
487 an inverse correlation between adsorption constant and plaque size (**Fig. 3**). This pattern is
488 consistent with previous findings in phage λ, where mutations in the host recognition protein J
489 that increased the adsorption constant led to reduced plaque size [17, 22]. Similar observations
490 were also made in phage U136B, where fast adsorbers often formed smaller plaques [56]. A
491 likely explanation for this is that rapid adsorption promotes local reinfection, trapping phages
492 at the focus of infection and preventing them from reaching uninfected regions of the bacterial
493 lawn [22].
494
495 Our findings identify adsorption and persistence as key life-history traits mediating
496 ΦX174 adaptation to different environmental conditions. The contrasting effects of different
497 adsorption constants across environments suggest ecological trade-offs that may drive
498 divergent selection in natural populations. For instance, sewage water, a major source of
499 phages, contains both a liquid phase where bacteria grow pelagically and a semi-solid phase
500 where bacteria form biofilms [57, 58]. High adsorption may be favoured in the liquid phase to
501 exploit transient host availability. In contrast, slow adsorption may be advantageous in biofilms
502 or host-rich environments to avoid attachment to already infected cells [17]. Low adsorption
503 could also be beneficial in particle-rich environments, where phages risk irreversible binding
504 to inert material [20, 59, 60]. Recurrent transitions between these environments may have
505 shaped the evolutionary plasticity of adsorption in ΦX174, where single-point mutations in the
506 F protein can lead to changes in adsorption with profound fitness consequences in different
507 environments.

508 The rapid decay of the ancestral ΦX174 in our experimental conditions, losing more
509 than 90% of infectious particles in less than two hours, prompts a fundamental question: how
510 does ΦX174 persist in natural environments where host cells may be absent or scarce for
511 extended periods? One possibility, supported by our results, is that ΦX174 populations
512 diversify through mutation, generating subpopulations of highly persistent variants. However,

increased persistence may come at a cost [3, 18, 61, 62]. In our experiments, increased persistence was consistently linked to enhanced adsorption, a combination that may be maladaptive in host-rich and structured environments due to superinfection and local trapping. Thus, phenotypic diversification may be an adaptive strategy allowing lytic phages to cope with environmental heterogeneity.

These findings have potential practical relevance. Phages with different life-history traits may be more or less suited for treating different types of infections, such as biofilm or bloodstream infections. Our results illustrate how experimental evolution can uncover key environmental trade-offs, which may inform the selection or engineering of phages for therapy. In addition, understanding how phage life-history traits evolve under different selective pressures is essential for anticipating phage evolutionary dynamics once they are administered to patients. Thus, experimental evolution serves not only as a valuable research approach but also as a practical tool to guide the development of safer, more effective, and more predictable phage-based therapies.

**Acknowledgements**

We acknowledge the Sequencing Service Team from the Max Planck Institute for Evolutionary Biology in Plön for performing the Sanger Sequencing. We thank Daniel Martens and Anja Baade for their support regarding lab logistics as well as the entire Microbial Population Biology Department for their support. We also want to thank David Rogers for helping with PCR troubleshooting and Eva Lievens and Stephen T. Abedon for the insightful discussions on viral life history evolution. MR, CB, and ORM were supported by the International Max-Planck Research School for Evolutionary Biology (IMPRS EvolBio).

**Funding**

The funding for this study was received from the Max Planck Society. Work in JLG lab was also supported by ERC starting grant 853323.

**Data availability**

All raw sequencing, plaque imaging, and counting data, used to generate figures Fig. 1, Fig. 2, Fig. 3, Fig. 4B, Fig. 5B and Fig. S2 is available under **10.5281/zenodo.1707622**. The code used for simulations and analysis is available on GitHub under https://github.com/OReyesMatte/Reuter_2025.

**Supplementary material**

All supplementary material is found in file "Supplementary.pdf". The file contains supplementary figures **Fig. S1-S9**, supplementary tables **Table S1-S13**, and **Supplementary Methods**.

**Conflicts of interest**

The authors declare no conflict of interest.

**Author Orchids**

Manuela Reuter: https://orcid.org/0009-0000-5191-3414

Michael Sieber: https://orcid.org/0000-0003-2703-3665

Octavio Reyes-Matte: https://orcid.org/0009-0006-7031-6213

Christopher Böhmker: https://orcid.org/0009-0003-0098-9816

Jordan Romeyer Dherbey: https://orcid.org/0000-0002-6125-1722

Frederic Bertels: https://orcid.org/0000-0001-6222-4139

Javier Lopez-Garrido: https://orcid.org/0000-0002-8907-502X

## References


1. Abedon ST, Hyman P, Thomas C. Experimental examination of bacteriophage latent-period evolution as a response to bacterial availability. *Appl Environ Microbiol* 2003;**69**:7499–7506. https://doi.org/10.1128/AEM.69.12.7499-7506.2003

2. Eshelman CM *et al*. Unrestricted migration favours virulent pathogens in experimental metapopulations: Evolutionary genetics of a rapacious life history. *Philosophical Transactions of the Royal Society B: Biological Sciences* 2010;**365**:2503–2513. https://doi.org/10.1098/rstb.2010.0066

3. Dessau M *et al*. Selective pressure causes an RNA virus to trade reproductive fitness for increased structural and thermal stability of a viral enzyme. *PLoS Genet* 2012;**8**:e1003102. https://doi.org/10.1371/journal.pgen.1003102

4. Heineman RH, Bull JJ. Testing optimality with experimental evolution: Lysis time in a bacteriophage. *Evolution (N Y)* 2007;**61**:1695–1709. https://doi.org/10.1111/j.1558-5646.2007.00132.x

5. DeLong JP *et al*. Towards an integrative view of virus phenotypes. *Nat Rev Microbiol* 2022;**20**:83–94. https://doi.org/10.1038/s41579-021-00612-w

6. Abedon ST. Impact of phage properties on bacterial survival. In: Adams HT (ed.), Contemporary Trends in Bacteriophage Research. Nova Science Publishers, Inc., 2009, 217–235.

7. Ellis EL, Delbrück M. The growth of bacteriophage. *J Gen Physiol* 1939;**22**:365–384. https://doi.org/10.1085/jgp.22.3.365

8. Delbrück M. Adsorption of bacteriophage under various physiological conditions of the host. *J Gen Physiol* 1940;**23**:631–642. https://doi.org/10.1085/jgp.23.5.631

9. Delbrück M. The growth of bacteriophage and lysis of the host. *J Gen Physiol* 1940;**23**:643–660. https://doi.org/10.1085/jgp.23.5.643

10. Suttle CA, Chen F. Mechanisms and rates of decay of marine viruses in seawater. *Appl Environ Microbiol* 1992;**58**:3721–3729. https://doi.org/10.1128/aem.58.11.3721-3729.1992

11. Abedon ST. Phage Ecology. In: Calendar R, Abedon ST (eds.), The bacteriophages. Oxford: Oxford University Press, 2006, 37–46.

12. Adams MH, Wassermann FE. Frequency distribution of phage release in the one-step growth experiment. *Virology* 1956;**2**:96–108. https://doi.org/10.1016/0042-6822(56)90079-4

13. Abedon ST. Kinetics of phage-mediated biocontrol of bacteria. *Foodborne Pathog Dis* 2009;**6**:807–815. https://doi.org/10.1089/fpd.2008.0242

599 14. Lindberg HM, McKean KA, Wang I-N. Phage fitness may help predict phage therapy
600 efficacy. *Bacteriophage* 2014;**4**:e964081.
601 https://doi.org/10.4161/21597073.2014.964081

602 15. Abedon S. Phage therapy pharmacology: Calculating phage dosing. In: Laskin A,
603 Gadd G, Sariaslani S (eds.), Advances in Applied Microbiology. Academic Press Inc.,
604 2011, 1–40.

605 16. Kowalska JD *et al*. Growing trend of fighting infections in aquaculture environment—
606 opportunities and challenges of phage therapy. *Antibiotics* 2020;**9**:301.
607 https://doi.org/10.3390/antibiotics9060301

608 17. Gallet R, Shao Y, Wang IN. High adsorption rate is detrimental to bacteriophage
609 fitness in a biofilm-like environment. *BMC Evol Biol* 2009;**9**:241.
610 https://doi.org/10.1186/1471-2148-9-241

611 18. Heineman RH, Brown SP. Experimental evolution of a bacteriophage virus reveals the
612 trajectory of adaptation across a fecundity/longevity trade-off. *PLoS One*
613 2012;**7**:e46322. https://doi.org/10.1371/journal.pone.0046322

614 19. Mäkelä K, Laanto E, Sundberg LR. Determinants in the phage life cycle: The dynamic
615 nature of ssDNA phage FLiP and host interactions under varying environmental
616 conditions and growth phases. *Environ Microbiol* 2024;**26**:e16670.
617 https://doi.org/10.1111/1462-2920.16670

618 20. Daniels LL, Wais AC. Virulence in phage populations infecting *Halobacterium*
619 *cutirubrum*. *FEMS Microbiol Ecol* 1998;**25**:129–134. https://doi.org/10.1016/S0168-
620 6496(97)00089-5

621 21. Shao Y, Wang IN. Bacteriophage adsorption rate and optimal lysis time. *Genetics*
622 2008;**180**:471–482. https://doi.org/10.1534/genetics.108.090100

623 22. Gallet R, Kannoly S, Wang IN. Effects of bacteriophage traits on plaque formation.
624 *BMC Microbiol* 2011;**11**:181. https://doi.org/10.1186/1471-2180-11-181

625 23. Bull JJ *et al*. Exceptional convergent evolution in a virus. *Genetics* 1997;**147**:1497–
626 1507. https://doi.org/https://doi.org/10.1093/genetics/147.4.1497

627 24. Wichman HA *et al*. Different trajectories of parallel evolution during viral adaptation.
628 *Science (1979)* 1999;**285**:422–424. https://doi.org/10.1126/science.285.5426.422

629 25. Crill WD, Wichman HA, Bull JJ. Evolutionary reversals during viral adaptation to
630 alternating hosts. *Genetics* 2000;**154**:27–37. https://doi.org/10.1093/genetics/154.1.27

631 26. Wichman HA, Brown CJ. Experimental evolution of viruses: *Microviridae* as a model
632 system. *Philosophical Transactions of the Royal Society B: Biological Sciences*
633 2010;**365**:2495–2501. https://doi.org/10.1098/rstb.2010.0053

634 27. Wichman HA, Millstein J, Bull JJ. Adaptive molecular evolution for 13,000 phage
635 generations: A possible arms race. *Genetics* 2005;**170**:19–31.
636 https://doi.org/10.1534/genetics.104.034488

637 28. Sanger F *et al*. The nucleotide sequence of bacteriophage φX174. *J Mol Biol*
638 1978;**125**:225–246. https://doi.org/10.1016/0022-2836(78)90346-7

639 29. Sinsheimer RL. A single-stranded deoxyribonucleic acid from bacteriophage φX174. *J*
640 *Mol Biol* 1959;**1**:43–53. https://doi.org/10.1016/S0022-2836(59)80006-1

641 30. Fane B. ΦX174 *et al*. the *Microviridae*. In: Calendar R (ed.), The Bacteriophages.
642 Oxford University Press, Inc., 2006, 129–145.

643 31. Baas PD. DNA replication of single-stranded *Escherichia coli* DNA phages. *Biochim*
644 *Biophys Acta* 1985;**825**:111–139. https://doi.org/10.1016/0167-4781(85)90096-X

645 32. McKenna R *et al*. Atomic structure of single-stranded DNA bacteriophage ΦX174 and
646 its functional implications. *Nature* 1992;**355**:137–143.
647 https://doi.org/10.1038/355137a0

648 33. Sun L *et al*. Icosahedral bacteriophage Φx174 forms a tail for DNA transport during
649 infection. *Nature* 2014;**505**:432–435. https://doi.org/10.1038/nature12816

650 34. Burgess AB. Studies on the proteins of ΦX174 II. The protein composition of the ΦX
651 coat. *Proceedings of the National Academy of Sciences* 1969;**64**:613–617.
652 https://doi.org/10.1073/pnas.64.2.613

653 35. Incardona NL, Selvidge L. Mechanism of adsorption and eclipse of bacteriophage
654 ΦX174 II. Attachment and eclipse with isolated *Escherichia coli* cell wall
655 lipopolysaccharide. *J Virol* 1973;**11**:775–782.

656 36. Incardona NL, Tuech JK, Murti G. Irreversible binding of phage ΦX174 to cell-bound
657 lipopolysaccharide receptors and release of virus-receptor complexes. *Biochemistry*
658 1985;**24**:6439–6446.

659 37. Sun Y *et al*. Structural changes of tailless bacteriophage ΦX174 during penetration of
660 bacterial cell walls. *Proceedings of the National Academy of Sciences*
661 2017;**114**:13708–13713. https://doi.org/10.1073/pnas.1716614114

662 38. Ilag LL *et al*. Calcium ion-induced structural changes in bacteriophage ΦX174.
663 *Journal of Molecular Biologie* 1994;**244**:291–300.
664 https://doi.org/10.1006/jmbi.1994.1730

665 39. Romeyer Dherbey J *et al*. Stepwise evolution of *E. coli* C and φX174 reveals
666 unexpected lipopolysaccharide (LPS) diversity. *Mol Biol Evol* 2023;**40**:msad154.
667 https://doi.org/10.1093/molbev/msad154

668 40. Biggs KRH *et al*. Ecological approach to understanding superinfection inhibition in
669 bacteriophage. *Viruses* 2021;**13**:1389. https://doi.org/10.3390/v13071389

670 41. Hyman P, Abedon ST. Practical methods for determining phage growth parameters.
671 In: Clokie MRJ, Kropinski AM (eds.), Methods in molecular biology, 1st ed. Totowa,
672 NJ: Humana Press, 2009, 175–202.

673 42. Berg S *et al*. ilastik: interactive machine learning for (bio)image analysis. *Nat Methods*
674 2019;**16**:1226–1232. https://doi.org/10.1038/s41592-019-0582-9

675 43. Virtanen P *et al*. SciPy 1.0: fundamental algorithms for scientific computing in Python.
676 *Nat Methods* 2020;**17**:261–272. https://doi.org/10.1038/s41592-019-0686-2

677 44. Van Der Walt S *et al*. scikit-image: Image processing in Python. *PeerJ* 2014;**2**:e453.
678 https://doi.org/10.7717/peerj.453

679 45. R Core Team. A language and environment for statistical computing. R Foundation
680 for Statistical Computing. 2022. Vienna, Austria, 2022.

681 46. Abedon ST. Detection of Bacteriophages: Phage Plaques. In: Harper DR et al. (eds.),
682 Bacteriophages: biology, technology, therapy. Springer Cham, 2021, 507–538.

683 47. Lee Y, Yin J. Detection of evolving viruses. *Nat Biotechnol* 1996;**14**:491–493.
684 https://doi.org/10.1038/nbt0496-491

685 48. Abedon ST, Yin J. Bacteriophage plaques: theory and analysis. In: Clokie MRJ,
686 Kropinski AM (eds.), Bacteriophages: Methods and Protocols, Volume 1: Isolation,
687 Characterization, and Interactions. Totowa, NJ: Humana Press, 2009, 161–174.

688 49. Fujimura R, Kaesberg P. The adsorption of bacteriophage ϕX174 to its host. *Biophys J*
689 1962;**2**:433–449. https://doi.org/10.1016/S0006-3495(62)86866-0

690 50. Bayer ME, Starkey TW. The adsorption of bacteriophage ΦX174 and its interaction
691 with *Escherichia coli*; a kinetic and morphological study. *Virology* 1972;**49**:236–256.
692 https://doi.org/10.1016/S0042-6822(72)80026-6

693 51. Van Der Avoort HGAM *et al*. Regions of incompatibility in single-stranded DNA
694 bacteriophages ΦX174 and G4. *J Virol* 1984;**50**:533–540.
695 https://doi.org/10.1128/jvi.50.2.533-540.1984

696 52. Wichman HA *et al*. Experimental evolution recapitulates natural evolution.
697 *Philosophical Transactions of the Royal Society B: Biological Sciences*
698 2000;**355**:1677–1684. https://doi.org/10.1098/rstb.2000.0731

699 53. Pepin KM, Domsic J, McKenna R. Genomic evolution in a virus under specific
700 selection for host recognition. *Infection, Genetics and Evolution* 2008;**8**:825–834.
701 https://doi.org/10.1016/j.meegid.2008.08.008

702 54. Lee KH *et al*. First-step mutations for adaptation at elevated temperature increase
703 capsid stability in a virus. *PLoS One* 2011;**6**:e25640.
704 https://doi.org/10.1371/journal.pone.0025640

705 55. Bull JJ, Badgett MR, Wichman HA. Big-benefit mutations in a bacteriophage inhibited
706 with heat. *Mol Biol Evol* 2000;**17**:942–950.
707 https://doi.org/10.1093/oxfordjournals.molbev.a026375

708 56. Burmeister AR *et al*. Experimental evolution of the TolC-receptor phage U136B
709 functionally identifies a tail fiber protein involved in adsorption through strong parallel
710 adaptation. *Appl Environ Microbiol* 2023;**89**:e0007923.
711 https://doi.org/10.1128/aem.00079-23

712 57. Jensen H, Biggs CA, Karunakaran E. The importance of sewer biofilms. *Wiley*
713 *Interdisciplinary Reviews: Water* 2016;**3**:487–494. https://doi.org/10.1002/wat2.1144

714 58. Balleste E *et al*. Bacteriophages in sewage: abundance, roles, and applications. *FEMS*
715 *microbes* 2022;**3**:xtac009. https://doi.org/10.1093/femsmc/xtac009

716 59. Harvey RW, Ryan JN. Use of PRD1 bacteriophage in groundwater viral transport,
717 inactivation, and attachment studies. *FEMS Microbiol Ecol* 2004;**49**:3–16.
718 https://doi.org/10.1016/j.femsec.2003.09.015

719 60. Richter Ł *et al*. Adsorption of bacteriophages on polypropylene labware affects the
720 reproducibility of phage research. *Sci Rep* 2021;**11**:7387.
721 https://doi.org/10.1038/s41598-021-86571-x

722 61. De Paepe M, Taddei F. Viruses' life history: Towards a mechanistic basis of a trade-
723 off between survival and reproduction among phages. *PLoS Biol* 2006;**4**:e193.
724 https://doi.org/10.1371/journal.pbio.0040193

725 62. García-Villada L, Drake JW. Experimental selection reveals a trade-off between
726 fecundity and lifespan in the coliphage Qß. *Open Biol* 2013;**3**:130043.
727 https://doi.org/10.1098/rsob.130043

728

729

730